Improved Ducted Fan Design for Small Flexible Wing Unmanned Air Vehicle

Radu Călin PAHONIE, Răzvan Viorel MIHAI, Radu BUŞE, and Mihai MIHĂILĂ-ANDRES

***Abstract*—Nowadays, equipment transportation or real time surveillance flights can be done with different types of UAVs (Unmanned Aerial Vehicles) ranging from quads to fixed wing vehicles and flexible winged ones. The purpose of this article is to build upon the research available in the field of small unmanned paramotor flexible winged gliders. Such a functional aerial vehicle has been built and initial flight data evaluation undertaken. In this paper we improve upon the initial design of the UAV and the flight behavior of its initial fan configuration. A new ducted structure is proposed and tested (numerically and experimental) for the electric fan propulsion system.**

***Index Terms*—flexible wing uav, ducted fan, small scale paramotor.**

I. Introduction

The world of small unmanned air vehicles is expanding at an incredible pace, with new designs available everyday and an ever-growing research enthusiasm. The main mission of such air vehicles has always remained closely related to surveillance in the sense that real time video image feed is a basic capability provided by any and all of the unmanned vehicles. To ensure a good quality of video transmission the flight speed tends to decrease and the stability of the air vehicle to increase. However there will be a considerable loss in operational range and maneuverability (see Table I).

To counter these drawbacks the team focused on the design of a small flexible wing paramotor that offers equilibrium between the fixed point level flight characteristics of quadcopters and their high quality video transmission and the high speed and autonomy of fixed wing UAVs.

A thorough investigation of the available research literature (such as [1-3]) gives enough reasons for choosing a small flexible wing paramotor to cover the mission requirements for higher operational flight time, high definition stable video transmission and increased payload capability. Its flexible wing in windy environments brings the advantages of gust alleviation and high lift without the need for sustained engine thrust and the configuration's pendulum stabile behavior brings another level of safety considering the role attitude and the coordinated turn maneuvers.

R. C. Pahonie is currently with the Doctoral School at the Military Technical Academy, 39-49 George Coşbuc Ave., Sector 5, 050141, Bucharest, Romania (e-mail: radu.pahonie@mta.ro).

R. V. Mihai is with the Integrated Systems of Aviation and Mechanics Department at the Military Technical Academy, 39-49 George Coşbuc Ave., Sector 5, 050141, Bucharest, Romania, and is also studying for his PhD thesis under the PhD Department of the Polytechnics University of Bucharest (e-mail: razvan.mihai@mta.ro).

R. Buşe is with the Base 90 of Aerial Transportation, Otopeni, Romania, and also studying for his PhD within the Doctoral School of the Military Technical Academy, 39-49 George Coşbuc Ave., Sector 5, 050141, Bucharest, Romania (e-mail: radu.buse@yahoo.com)

M. Mihăilă-Andres is the current Vice-dean for Research in the Integrated Systems of Aviation and Mechanics Department of the Military Technical Academy, 39-49 George Coşbuc Ave., Sector 5, 050141, Bucharest, Romania (e-mail: mihai.mihaila@mta.ro).

TABLE I. MISSION CAPABILITIES ASSESSMENT FOR DIFFERENT CONFIGURATION UAVS

UAV	Mission capabilities					
	Speed	Video transmission	Autonomy	Maneuverability	High winds behavior	Lift
Quad	0	2	0	1	1	0
Fixed wing	2	0	1	2	0	1
Flexible wing paramotor	1	1	2	0	2	2

A seriously advantageous aspect of the powered flexible wings or paramotors, is their tendency to fly at a constant airspeed whether in an upper trajectory or on descent, or even flying straight-and-level. Not only is the paramotors speed constant, but they have pendulum stability as well, due to the mass of the airframe suspended significantly below the canopy. This allows the wing to maintain a safe roll attitude and effectively turn in a coordinated manner when the steering arms are deflected. One of the challenges of flying these aircraft is the necessity of controlling altitude with thrust, and direction with asymmetric drag [1].

The following table (Table II) highlights the small scale paramotor functional model before the design modifications:

TABLE II. SMALL SCALE PARAMOTOR FUNCTIONAL MODEL DESIGN

Wing	
Wing span: 3.9 m *Deflated surface*: 2.53 m^2 *Inflated surface*: 3.05 m^2 *Number of cells*: 25 *Ties* : 25/50 daN *Weight*: 140 g *Maximum load*: 8 kg	 Figure 1. The wing of the paramotor
Body *Length*: 512 mm *Width:* 425 mm *Height:* 700 mm *Total weight*: 3260 g	 Figure 2. The complete structure of the paramotor

Digital Object Identifier 10.32754/JMT.2018.1.06

II. Theoretical Considerations

The autonomous control relies on the paramotor dynamics. The equations describing the flight dynamics depend on the aerodynamic coefficients, thus the model that needs to be modeled can only be constructed after having a physical reliable model. In this chapter we present the improved design of our paramotor, with an initial design of the structure that can be seen in Figure 3 below that was flight tested under varied conditions.

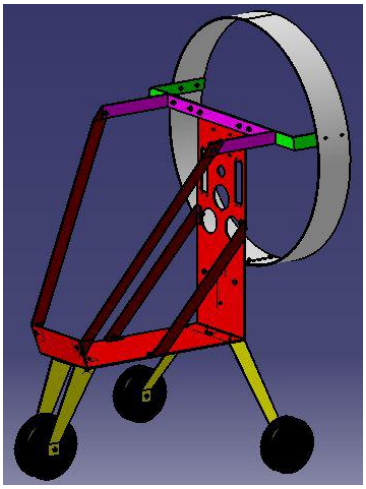

Figure 3. The first revision of the paramotor design model

The front surface of the duct is subjected to the drag force, given by the flowing air in case of a straight and uniform level flight.

$$R = \frac{1}{2}\rho_{air} V_{\infty}^2 2\pi r_{duct} C_x \quad (1)$$

A high amplitude oscillation of the tube's upper surface (the area between 90° to 180°) was apparent during the experimental flights. Large vibrations were induced to the paramotor frame that are harmful and can damage its propulsion system. An important aspect to state is that the materials that this structure was built with are as follows: wheels – rubber, frame and landing gear – aluminum alloy A6061, rotor duct – Plexiglas.

The eigenvalue and eigenvector problem that needs to be solved for this mode-frequency analysis has the theoretical form as follows:

$$[K]\{\varnothing_i\} = \lambda_i [M]\{\varnothing_i\}, \quad (2)$$

where [K] is the structural matrix, [M] is the mass matrix, $\{Q_i\}$ is the eigenvector and λ_i is the eigenvalue [4].

The initiation of buckling is determined by the tube's fasten points to the paramotor frame as well as the Plexiglas material characteristics. Thus, we considered a different grip on the paramotor frame by dividing the free portion of the tube (the portion where the frame is overlapping the tube was excluded) into three equal arc lengths. Finally, the positions on the tube, where the three points where fastened are at 0°, 126° and 234°.

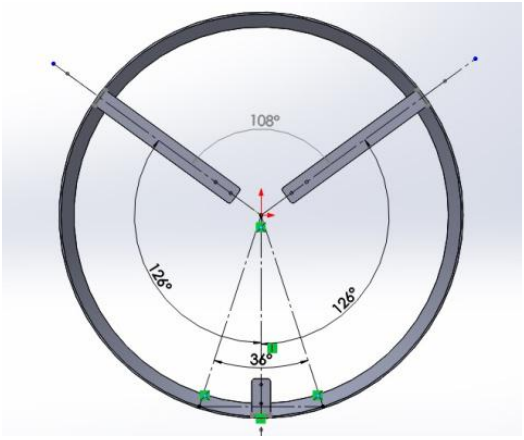

Figure 4. The tube fasten points locations

By applying this constructive solution, a loading symmetry was attempted in order to constrain the duct to act symmetrically after the excitation is applied.

III. Numerical Simulation

The experimental data from the accelerometer analysis was used as comparative basis for the numerical study. After constructing the CAD of the paramotor in Solidworks and exporting it as an iges file into Ansys [9], the material characteristics of the structure were defined. Using the properties found in references [6] and [7] the Plexiglas and the aviation grade aluminum alloy A6061 were defined as new materials and imported into the modal simulation environment.

The properties of both materials are presented in Table III.

TABLE III. Material Characteristics Implemented in Ansys

Properties	**Plexiglas**	**Al A6061**
Density	1.19 g/cm^3	2.7 g/cm^3
Tensile strength	80 MPa	310 MPa
Modulus of elasticity	3300 MPa	68.9 GPa
Shear modulus	1700 MPa	26 GPa
Poisson's ratio	0.37	0.33
Elongation at break	5.5%	12%

Only the duct and its aluminum frame arms were considered for this analysis. A static structure simulation was first run with respect to the specific weights that act on the structure itself, weights given mostly by the batteries, the servos, the engine and the surveillance equipment. The total weight of the system does not reach the equivalent mass of 5 kg, specifically is close to 44 N. Imposing the loads as system weight and air resistance on the inner surface of the duct ring, the aluminum arms were constrained with zero degrees of freedom. The meshing of the frame arms and duct were done initially with quad volume elements to account for the complexity of the deformation, but due to the fact that Artemis [12] cannot process quad elements only triangular ones, the entire mesh was changed. The number of used elements was of about 20000 totaling some 10000 nodes.

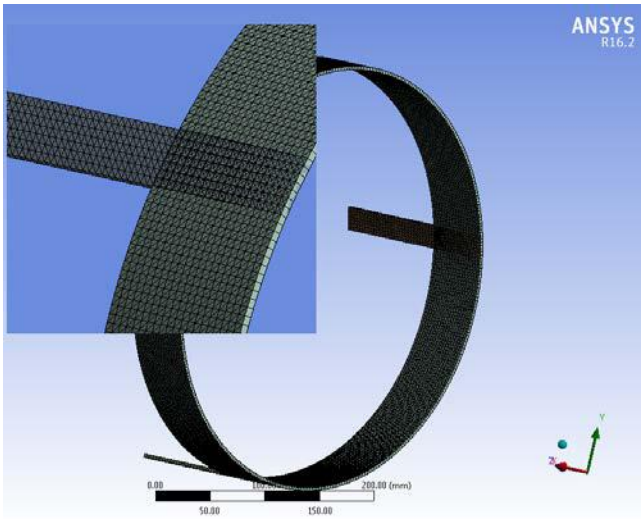

Figure 5. Meshing the duct with triangle elements

The analysis considered the duct as a Plexiglas isotropic material [8], therefore a simplification was made to the geometry considering triangular surface elements. However an element size restriction has been imposed on the elements and that is to not be greater that 3 mm in any dimension. This constraint greatly improved the mesh. Six natural frequencies and mode shapes were determined after the analysis as Figure 6 illustrates.

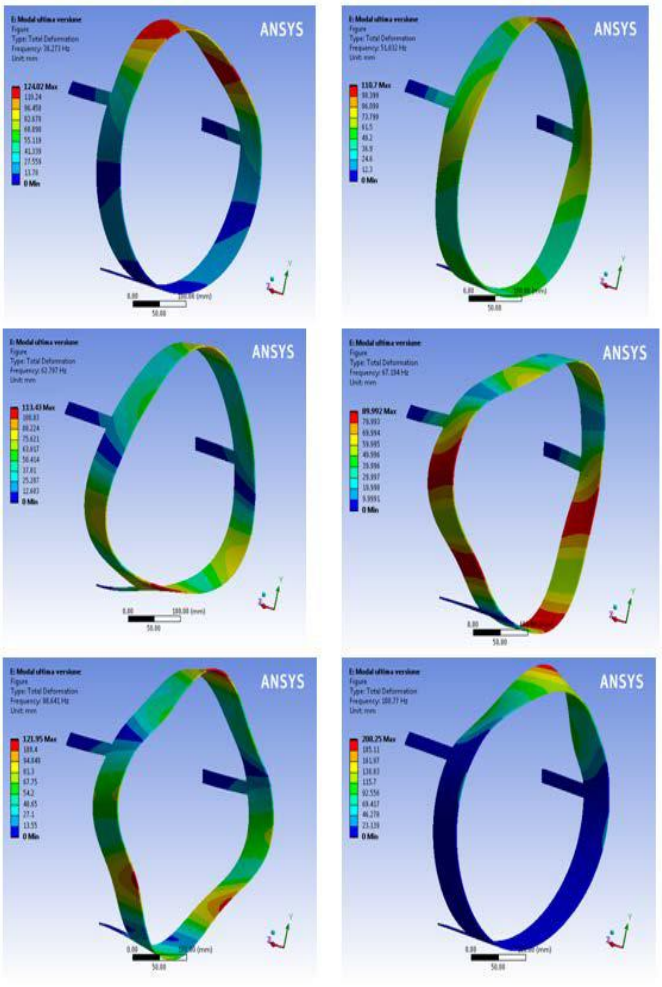

Figure 6. Mode shapes and natural frequency for the duct with Plexiglas material and aluminum alloy frame

The determined natural frequencies had values that were considerably below the 130 Hz range (Table IV), the frequency value range introduced by the rotating propeller to the structure; therefore it became obvious that a structural design change was needed.

TABLE IV. DETERMINED FREQUENCIES AFTER MODAL ANALYSIS BEFORE AND AFTER THE DESIGN CHANGE OF THE DUCT STRUCTURE

Mode	Before design change Frequency (Hz)	After design change Frequency (Hz)
1.	38.273	126.59
2.	51.032	142.22
3.	62.797	142.25
4.	67.194	191.24
5.	98.641	194.51
6.	100.77	194.64

The first idea was to introduce another three support arms and the second was to change the Plexiglas material to an aluminum alloy. Implementing the first idea into the analysis meant regenerating the geometry, re-meshing (see Figure 7) and retracing the analysis steps.

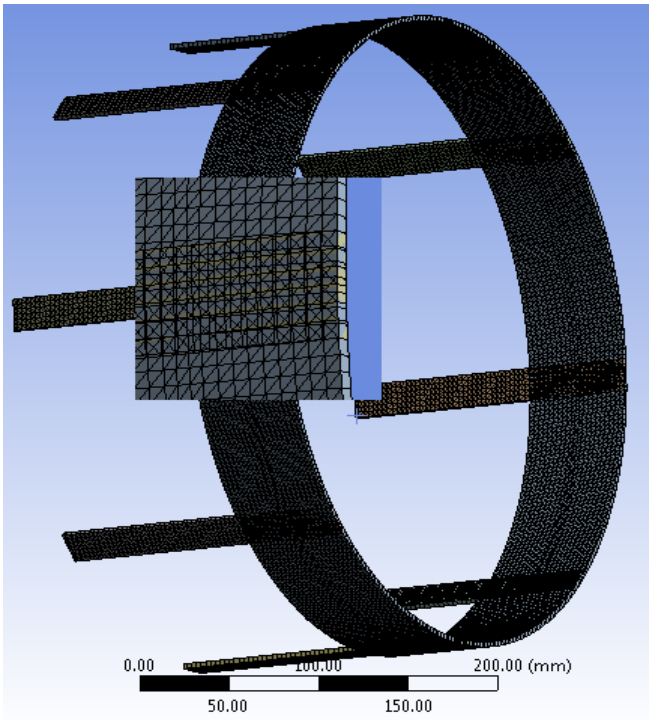

Figure 7. Meshing the improved duct with triangle elements and zoom in on elemental coupling

But the results were deemed satisfactory as the natural frequencies, for the most part, surpassed the critical 130 Hz. The only one under the limit was the first frequency. Still, considering the fact that structural arms are riveted to the Plexiglas duct with four rivets on two rows, that were not taken into consideration in the numerical geometry model or even in the analysis, this critical frequency value can be easily exceeded. Figure 8 below shows the mode shapes for the duct with six structural arms and the exaggerated view of the deformations that underline the critical areas.

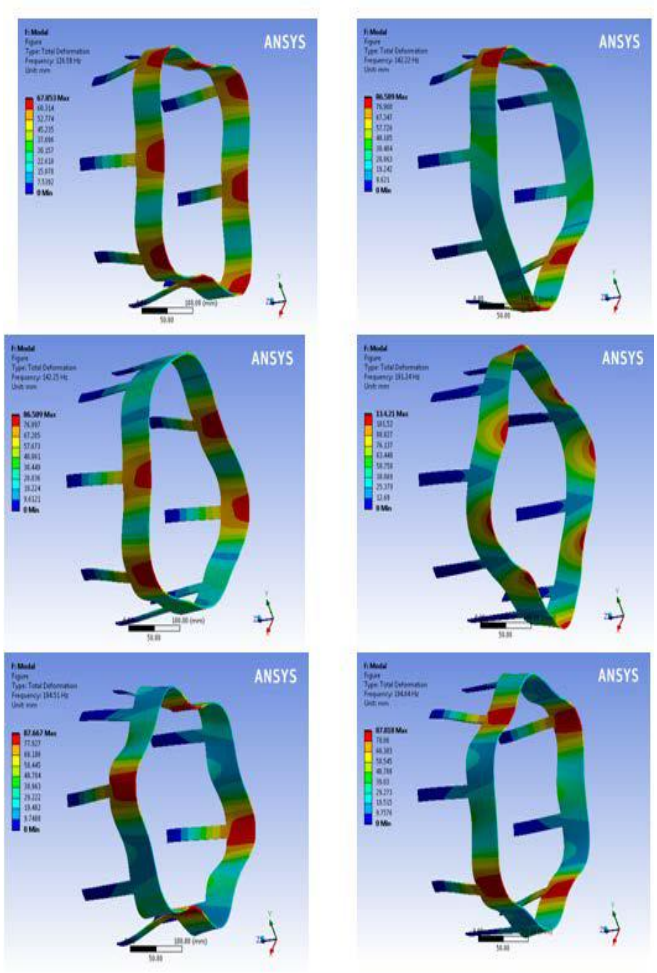

Figure 8. Mode shapes and natural frequency for the duct with Plexiglas material and aluminum alloy frame

IV. Experimental Procedure and Data

After the numerical simulation it became apparent that experimental data were needed in order to validate the design. Therefore a fixing rig was constructed on a metal table to hold the Plexiglas duct in place via the structural aluminum arms. The Ansys geometry was exported to the Femtools software [10] for another modal analysis that would offer an automatic pole section based on a stabilization chart. Although this is a global method, it allowed for the accurate placing of the sensors on the modal (see Figure 9).

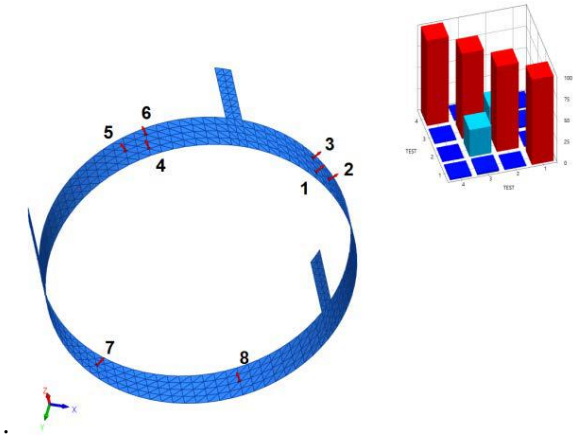

Figure 9. Positioning the 8 sensors using an auto generated stabilization chart (top right view) from the Femtools software

A number of eight Dytran accelerometers, with a sensitivity of 100 mV/g and 1.1 g in weight, were placed on the Plexiglas duct according to the data gathered from the Femtools. They were each connected to MX840B quantum data acquisition board capable of 40 kS/s on every channel and an active low pass filter (see Figure 10).

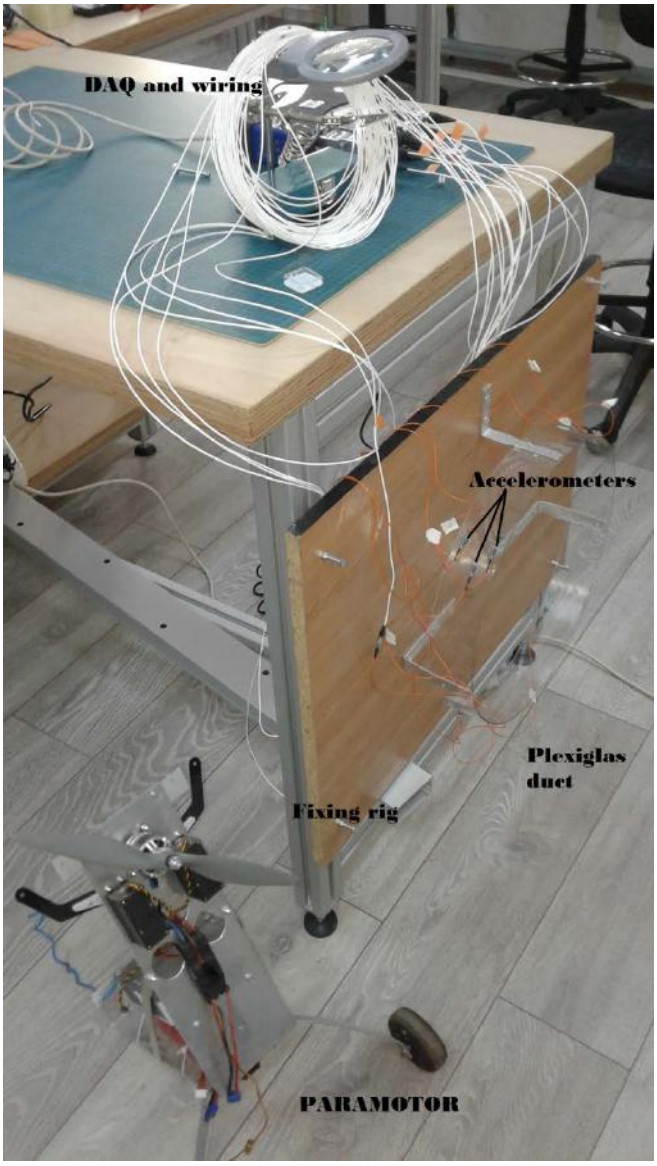

Figure 10. Experimental setup for modal analysis of Plexiglas duct with named components

The data during the experiment were gathered with the Catman software [11] with a capability of up to 12 MS/s and viewed in real time. After the data was collected, Artemis software was used to correlate the data with the geometry model. A frequency domain decomposition chart was generated that highlighted the singular values of the spectral densities for the test setup and the peak dB values on the graph were identified with their frequencies as natural modes of the duct. Those frequencies values are presented in Table V along the numerical generated values for comparison purposes and in Figure 11 for visual confirmation.

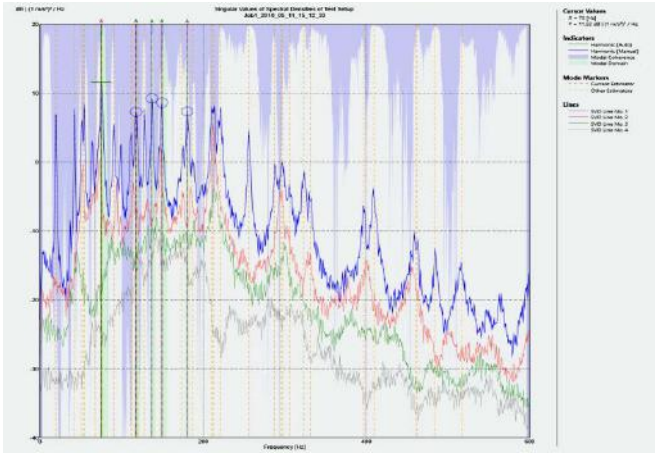

Figure 11. Harmonics generated by Artemis software after sensor data and their duct position correlation

TABLE V. DETERMINED FREQUENCIES AFTER MODAL EXPERIMENTAL ANALYSIS BEFORE THE DESIGN CHANGE OF THE DUCT STRUCTURE

Mode	Before design change Frequency (Hz) Numerical determination	After design change Frequency (Hz) Experimental determination/Damping %
1.	38.273	40.547 / 2.741
2.	51.032	52.22 / 2.127
3.	62.797	64.25 / 4.149
4.	67.194	69.24 / 1.435
5.	98.641	104.51 / 2.667
6.	100.77	114.64 / 1.571

The obtained values offer the validation needed for the numerical procedure applied for the improvement of the design.

V. LANDING GEAR DESIGN AND IMPROVEMENTS

The geometry and the aluminum alloy of the landing gear showed a higher than expected elastic behavior, that proved to be detrimental to the landing procedure. This behavior is useful during high approach speed landings, but most of the time tends to destabilize the paramotor on its ground maneuvers, especially if the first runway touchdown is made with only one wheel.

First approach, due to weight considerations, was to build the loading gear structure out of an aluminum alloy band of 2 mm in thickness. After observing the paramotors flight behavior we replaced the aluminum with an OL37 steel with a 1.25 mm in thickness. The added weight penalty was of about 93 g, due to the difference in material densities.

Another aspect in which the landing gear design was improved is related to the paramotor longitudinal stability on landing, more precise, on the pitch axis.

To improve paramotor stability both at landing and during taxiing, the angle between MLG (Main Landing Gear) and ALG (Auxiliary Landing Gear) was increased from 0° to 30° with respect to the vertical line. This can be seen in Figure 12.

A 2.5° angle was also established between the horizontal axes lines of the MLG and ALG wheels.

The stability on the roll axis was also be improved by increasing the wheelbase between the landing gear components. In this respect, on the one hand, the angle between ALG with respect to the vertical plane was augmented from 30° to 45° and on the other, the distance between ALG wheels was enlarged from 316 mm to 402 mm.

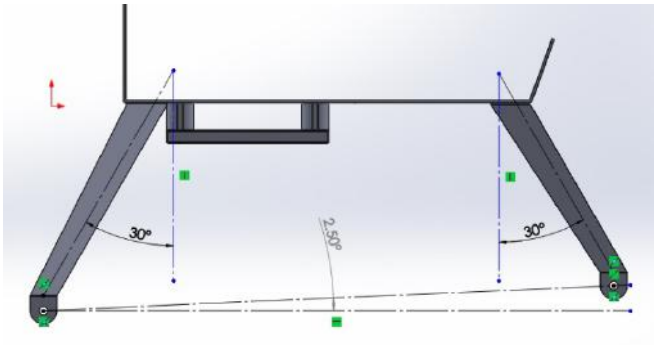

Figure°12. Landing gear angle modifications with respect to the vertical line

After structurally applying the geometrical modifications, the overall mass of the paramotor frame was increased by 35.7 g (Figure 13).

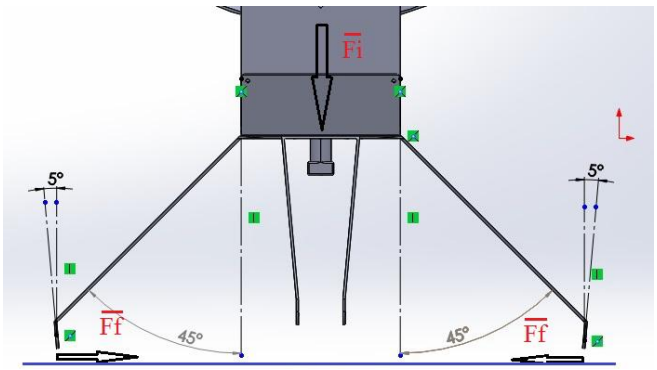

Figure°13. Bottom view of the paramotor frame

In order to ensure a greater stability for the paramotor frame when running on the runway, the wheel angles must be convex.

From a top viewing perspective, the ALG wheels angle must have a positive value, because when landing ALG are under impact loading and their behavior has to be elastic to dampen the impact. That will increase the angle between the two ALG with a value conditioned by the friction force between the wheels and the runway surface and also by the inertial force of the paramotor.

An initial value of 5º was set between the horizontal axis of the MLG and LAG that will also improve the runway maneuvers by lowering the winds angle of incidence. Further studies need to be carried out in order to set the required angle according to the paramotor weight variations and different landing maneuvers.

VI. CONCLUSION

In this paper, the design of a small scale paramotor which has been built for military transport and surveillance operations was improved based on experimental flight tests, numerical and experimental determination. The latter paramotor design was compared with the former one both geometrically as well as functional.

The first paramotor structure improvement regards the propeller duct and frame connecting arms. The vibration inducing and stability degrading three-beam structure has been modified, after a software FEM numerical simulation, into a six-beam structure. This was done after the experimental validation of the numerical applied procedure. Eight accelerometers and a modern data acquisition board and software were used to obtained quality data.

The numerical analysis determined the natural frequencies and modes for the unmodified design and for the improved one, via the Ansys and Femtools software. Material characteristics were defined for both materials used, the geometries were drawn and redrawn according to the specific modifications and assumptions and a fine mesh of the model was generated. The meshing took into account the compatibility between the experimental and numerical software utilized, and employed surface triangular elements of no more than 3 mm in length. Six natural frequencies were determined for both geometries under the same material characteristics of the parts. After changing all the materials to aluminum alloy A6061 for all the parts, the natural frequency of the system would undoubtedly rise at the penalty of a growing mass. If the structure had been redesigned out of an aluminum alloy its mass would be around the 700 g, as against the proposed six-beam design mass of 480 g.

Another aspect is the work performed improving the landing gear design that benefited the paramotors longitudinal stability on landing, more precisely on the pitch axis.

An initial value of 5º was set between the horizontal axis of the MLG and LAG that will also improve the runway maneuvers by lowering the winds angle of incidence.

Further research must be conducted in order to obtain precise values for paramotor's convergent duct geometry, which will increase its flight speed. An optimal value for the ALG wheels falling angle influences the stability when running the runway, this being important for the integrity of the transported first aid kit load.

ACKNOWLEDGMENT

This work was supported by the Doctoral School and the Integrated Systems of Aviation and Mechanics Department of the Military Technical Academyand the PhD Department of the Polytechnics University of Bucharest.

REFERENCES

[1] J. R. Chambers, *Longitudinal Dynamic Modelling and Control of Powered Parachute Aircraft*, M.S. thesis, Department of Mechanical Engineering Committee, Rochester Institute of Technology, Rochester, NY, 2007.

[2] D. Carter, S. George, P. Hattis, L. Singh, S. Tavan, "Autonomous Guidance, Navigation, and Control of Large Parafoils," 18th AIAA Aerodynamic Decelerator Systems Technology Conference and Seminar, Munich, Germany, 23-26 May 2005. doi: 10.2514/6.2005-1643

[3] R. V. Mihai, C. Vidan, R.-C. Pahonie, P. Matei, A.-M. Stoica, I. Adochiei, *A semi-autonomous small scale paramotor used for medical emergency situations*, in Proc. 2015 E-Health and Bioengineering Conference (EHB), 19-21 Nov. 2015. doi: 10.1109/EHB.2015.7391531

[4] R. W. Clough, J. Penzien, *Dynamics of Structures*, 2nd ed., McGraw-Hill College, NY, 1993.

[5] J. D. Anderson Jr., *Fundamentals of Aerodynamics*, McGraw-Hill Inc., US, 1984.

[6] www.plexiglass.de, "Properties of Plexiglas".

[7] asm.matweb.com, Aerospace Specification Metals Inc., Aluminum 6061-T6 properties.

[8] M. Mihaila-Andres, I. Fuiorea, "Aeroelastic analysis of rotorcraft using Ansys," in Proc. ICMT'13, Brno, Czech Republic, 2013, pp. 779-788.

[9] Ansys help documentation, 2015

[10] Femtools help documentation, 2015

[11] Catman help documentation, 2015

[12] Artemis help documentation, 2015